The Link between Membrane Composition and Permeability to Drugs

Chi Hang Tse,†,‡ Jeffrey Comer,¶ Yi Wang,*,†,‡ and Christophe Chipot*,§,||,⊥

†Shenzhen Research Institute, The Chinese University of Hong Kong, Shatin, Hong Kong SAR, China

‡Department of Physics, The Chinese University of Hong Kong, Shatin, Hong Kong SAR, China
¶Institute of Computational Comparative Medicine and Nanotechnology Innovation Center of
Kansas State, Department of Anatomy and Physiology, Kansas State University, Manhattan,
Kansas 66506

§Laboratoire International Associé Centre National de la Recherche Scientifique et University of Illinois at Urbana-Champaign, Unité Mixte de Recherche n°7565, Université de Lorraine, B.P. 70239, 54506 Vandœuvre-lès-Nancy cedex, France

||Theoretical and Computational Biophysics Group, Beckman Institute for Advanced Science and Technology, University of Illinois at Urbana-Champaign, 405 North Mathews Avenue, Urbana, Illinois 61801

⊥Department of Physics, University of Illinois at Urbana-Champaign, 1110 West Green Street,

Urbana, Illinois 61801

E-mail: yiwang@cuhk.edu.hk; chipot@ks.uiuc.edu

Abstract

Prediction of membrane permeability to small molecules represents an important aspect of drug discovery. First-principle calculations of this quantity require an accurate description of both the thermodynamics and kinetics that underlie translocation of the permeant across the lipid bilayer. In this contribution, the membrane permeability to three drugs, or drug-like molecules, namely, 9-anthroic acid (ANA), 2',3'-dideoxyadenosine (DDA) and hydrocortisone (HYL) are estimated in a pure 1-palmitoyl-2-oleoyl-phosphatidylcholine (POPC) and in a POPC:cholesterol (2:1) mixture. On the basis of independent $2-5-\mu s$ free-energy calculations combined with a time-fractional Smoluchowski determination of the diffusivity, the estimated membrane permeabilities to these chemically diverse permeants fall within an order of magnitude from the experimental values obtained in egg lecithin bilayers, with the exception of HYL in pure POPC. This exception is particularly interesting because the calculated permeability of the sterol-rich bilayer to HYL, in close agreement with the experimental value, is about 600 times lower than that of the pure POPC bilayer to HYL. In contrast, the permeabilities to ANA and DDA differ by less than a factor of ten between the pure POPC and POPC: cholesterol bilayers, although the trend of a lower permeability in the sterol-rich bilayer holds for all permeants. The unusual behavior of HYL, a large, amphiphilic compound, may be linked with the longer-range perturbation of the lipid bilayer it induces, compared to ANA and DDA, suggestive of a possibly different translocation mechanism. We find that the tendency of lower permeabilities of the POPC:cholesterol bilayer relative to those of the pure POPC one is a consequence of increased free-energy barriers. Furthermore, our fractional-diffusion model predicts a slightly more pronounced deviation from classical diffusion for the translocation of the permeants through the sterol-rich medium, relative to the pure-phospholipid bilayer, which also contributes to a lower permeability of the former. Beyond reporting accurate estimates of the membrane permeability, the present contribution also demonstrates that rigorous free-energy calculations and a fractional-diffusion model is the key that reveals the molecular phenomena linking the composition of a membrane to its permeability to drugs.

Introduction

Drug discovery is a time consuming and expensive process.¹ The cost of drug development is estimated to be on the order of \$2.6 billion US dollars, and has increased by 150% since the last decade.¹ Approximately 75% of this cost can be attributed to failure at different stages in the drug-discovery pipeline. Addressing high drug-attrition rate remains in large measure a key challenge for the pharmaceutical industry. Promising drug candidates, which, in the early stage of drug discovery, exhibit a strong affinity towards the target of interest, may fail at a later stage due to cytotoxicity,² poor bioavailability,³ or pharmacokinetics-related issues.³ A priori knowledge of such key properties of the drug candidate are crucial to reduce unnecessary organic syntheses, as well as expensive assays and clinical trials.

The permeation rate of the drug candidate is an important pharmacokinetic quantity for the description of the absorption and distribution of the orally administered drug inside the body. In practice, in an industrial setting, high-throughput pharmacokinetic experiments relying on parallel artificial membrane permeability assay (PAMPA), as well as Caco-2⁴ and Madin Darby canine kidney^{5,6} (MDCK) cell lines (and the variant of the latter, with low expression of endogenous canine Pgp transporter, referred to as Ralph Russ canine kidney, or RRCK) are used to measure the membrane permeability and have helped reduce the pharmacokinetically related drug attrition rates from 40% to 10%. However, these experimental studies mostly measure the permeability in an indirect way, employing, for instance, the micropipette-aspiration technique to determine the mechanical properties of a lipid vesicle immersed in an aqueous solution containing the permeant.⁷ Moreover, the assay still requires organic synthesis of the substrate. To optimize phamacokinetics prior to costly syntheses, an accurate, predictive permeability model is required to relate the physicochemical properties of the drug to those of the lipid bilayer. There have been numerous experimental studies aimed at developing an empirical model with different determinants, such as permeant size 8,9 solute hydrophobicity,9 solute volume, 10 membrane fluidity, 11 cholesterol content 12 and chain ordering 13 in a membrane bilayer.

Such empirical models lack a solid theoretical foundation and are not robust enough to be

applied universally. ¹⁴ Statistical-mechanics-based simulations, e.g., molecular dynamics (MD), provide a more robust approach to membrane-permeability calculations. ^{15–18} A popular framework that makes use of MD trajectories to predict the membrane permeability is the inhomogeneous solubility–diffusion model, which relates the resistance to permeation ($P_{\rm m}$) to the integral of the position dependent diffusivity D(z) of substrate and the potential mean force (PMF), w(z), that underlies permeant translocation. ¹⁹

$$R = \frac{1}{P_{\rm m}} = \int_{-\frac{L}{2}}^{+\frac{L}{2}} dz \, \frac{\exp[\beta w(z)]}{D(z)} \tag{1}$$

 $\beta=1/k_{\rm B}T$, where T is the temperature and $k_{\rm B}$ is the Boltzmann constant. z is the transition coordinate, defined as the projection onto the z-axis of Cartesian space of the Euclidean distance separating the center of mass (COM) of the permeant from that of the lipid bilayer. Because of the exponential factor in equation 1, accurate evaluation of w(z) is crucial. It ought to be noted that an error as small as $1.4k_{\rm B}T$ in the free-energy calculation is tantamount to an error in the membrane permeability of one order of magnitude. However, an accurate free-energy calculation remains extremely challenging for two reasons, namely (i) the rudimentary nature of pairwise additive force fields for drug molecules, and (ii) the notorious slow convergence of importance-sampling simulations like umbrella sampling, 20 adaptive biasing force (ABF), 21,22 or metadynamics. 23

There are a number of routes towards the estimation of the diffusivity, D(z), from MD simulations, including the Einstein-Smoluchowski equation based on the mean squared displacement, ²⁴ or its velocity-autocorrelation function variant, ²⁴ and the generalized Langevin equation for a harmonic oscillator. ^{25–27} A comparative study has shown that the Einstein-Smoluchowski route is unreliable for transition coordinates with large variations of the free energy. ²⁸ Conversely, application of the generalized Langevin equation has proven to perform better by unbiasing the influence of systematic force acting along the transition coordinate. ²⁸ However, it has been reported that an accurate representation of D(z) would require separate trajectories to be generated in the framework of an overdamped Langevin regime, ²⁶ thereby calling for additional computational resources. Recently, a new approach for the determination of the position-dependent diffusivity has been put

forth and rests upon a Bayesian-inference strategy, 29 allowing D(z) and w(z) to be determined in a consistent fashion from the same biased trajectory. This approach has proven well-suited to handle the time-dependent bias of ABF calculations.

Aside from the choice of a suitable method for the determination of the position-dependent diffusivity from biased simulations, another aspect of the methodology ought to be considered, namely the limit of the validity of the model. While permeation events have been traditionally examined in the framework of the solubility-diffusion model, under the assumption of continuous-time random walk, ¹⁹ recent theoretical investigations have demonstrated that translocation of small substrates across a lipid bilayer, as measured along the rudimentary coarse variable z, does not obey classical diffusion. ^{30,31} In fact, permeation along the normal to the bilayer has been shown to follow a subdiffusive regime, whereby the mean squared displacement satisfies a power law, $\langle z^2 \rangle \sim K_\alpha t^{\alpha(z)}$, where t is the time and $0 < \alpha(z) < 1$ is the fractional order of the diffusivity. $\alpha = 1$ corresponds to classical diffusion and can be observed in the aqueous phase, sufficiently far from the membrane interfacial region. For values of z within the hydrophobic core of bilayers formed by lipids like 1-palmitoy1-2-oleoy1-phosphatidylcholine (POPC), α can be as low as 0.7, which is a signature of subdiffusion. ^{30,31}

The origin of subdiffusion can be found in the slow collective motions of the lipids in the membrane, resulting in local fluctuations of the atomic density inside the bilayer. The high-density region causes immobility of the permeant over a significant timescale. In turn, displacement of the substrate is facilitated by the spontaneous formation of transient voids over timescales comparable to that of permeation itself.³⁰ The subdiffusive behavior is modeled by means of a time-fractional Smoluchowski equation, wherein the first-order time derivative of the classical form of the Smoluchowski equation is replaced by a fractional derivative with a fractional order $\alpha(z)$ that depends on the position of the permeant relative to the membrane: 30,31

$$\partial_t^{\alpha(z)}c(z,t) = \partial_z[K_\alpha(z) - \beta K_\alpha(z) - \beta K_\alpha F(z,t)]c(z,t). \tag{2}$$

where $K_{\alpha}(z)$ is the fractional diffusivity, F(z,t) is the deterministic force, which obeys F(z,t)

 $=\partial_z w(z)$ for a conservative system, and c(z,t) is the concentration of the permeant. This sub-diffusive model has been employed to estimate the membrane permeability to a series of short-chain alcohols, revealing a trend very similar to that found experimentally. Theoretical efforts to determine the membrane permeability to large, drug-like molecules, e.g., hydrocortisone, using either a classical-diffusion or a subdiffusive model, remain, however, scarce. In the present work, we examine the influence of cholesterol on the membrane permeability of three drug or drug-like compounds, namely 9-anthroic acid (ANA), also referred to as anthracene-9-carboxylic acid, 2',3'-dideoxyadenosine (DDA), and hydrocortisone (HYL). Cholesterol is an essential component of mammalian cellular membranes, responsible for modulating their physicochemical properties. In particular, it is now well understood that cholesterol modulates the fluidity of lipid bilayers and confers to the alkyl chains a higher directional order. A host of experimental studies have shown that an increase in cholesterol concentration in the membrane reduces the permeability of the latter to small molecules, like water, oxygen, glucose by a factor of 2–4. In 1.12.36,37

In a recent computational study of the translocation of small solutes from water to the membrane, a decrease of the partitioning was observed as the cholesterol concentration increases. ³⁸ This study, however, focuses on the thermodynamics of translocation, and, thus, does not provide an estimation of the membrane permeability. Theoretical investigations of the correlation between cholesterol content and membrane permeability remain admittedly scarce. On the other hand, simulations have shown that cholesterol reduces the free volume in lipid bilayers, ^{37,39} which suggests it may impact the diffusive properties of the substrate embodied in its fractional order, $\alpha(z)$, and fractional diffusivity, $K_{\alpha}(z)$. In the following section, we outline the theoretical background of membrane permeability calculations in a subdiffusive regime, and detail the protocols of the simulations.

Methods

Theoretical Underpinnings

The fractional, position-dependent diffusivity, $K_{\alpha}(z)$, can be determined in a Bayesian-inference approach. ³⁰ The trajectory of the permeant, Z(t), and the reversible work, w(z), incurred in membrane permeation can be readily obtained from a free-energy calculation with a time-dependent bias, as is the case with the ABF algorithm. ²² Starting with an initial guess of $K_{\alpha}(z)$ and $\alpha(z)$, the likelihood of the observed trajectory is given by,

$$P[Z(t)|K_{\alpha}(z),\alpha(z)] = \prod_{j} P[Z(t_{j} + \Delta t)|Z(t_{j}),K_{\alpha}(z),\alpha(z)]$$
(3)

where Z(t) represents the trajectory of the permeant along z during the simulation, which may be subject to an enhanced sampling method, and Δt is the time interval in the discretization scheme. The likelihood is the product of all the conditional probabilities of a displacement at time t_j , given the current estimate of $K_{\alpha}(z)$ and $\alpha(z)$. The goal is to find $K_{\alpha}(z)$ and $\alpha(z)$ that maximize the posterior probability, $P[K_{\alpha}(z), \alpha(z)|Z(t)]$. The posterior probability can then be related with the likelihood through the Bayes theorem,

$$P[K_{\alpha}(z), \alpha(z)|z(t)] = P[Z(t)|K_{\alpha}(z), \alpha(z)]P_{\text{prior}}[K_{\alpha}(z)]$$
(4)

Our model introduces a prior, P_{prior} , which is the product of priors that implement an assumption of scale invariance and smoothness of the diffusivity, ³⁰

$$\begin{cases}
p_{\text{smooth}}[K_{\alpha}(z)] = \prod_{i>1} \exp\left(-\frac{[K_{\alpha}(z_i) - K_{\alpha}(z_{i-1})]^2}{2h^2\epsilon^2}\right) \\
p_{\text{scale}}[K_{\alpha}(z)] = \prod_{i} \frac{1}{K_{\alpha}(z_i)}
\end{cases} (5)$$

In the present fractional-diffusivity model, $P[Z(t_j + \Delta t)|Z(t_j), K_{\alpha}(z), \alpha(z)]$ is computed using the Crank–Nicolson finite-difference algorithm, ^{40,41} and a first-order approximation of the frac-

tional derivative in the Caputo sense, 42

$$\partial_t^{\alpha} f(t) \sim \frac{1}{(1-\alpha)\Gamma(1-\alpha)\tau^{\alpha}} \sum_{j=2}^{t/\tau} \omega_j^{(\alpha)} \left[f(t-j\tau+\tau) - f(t-j\tau) \right]$$
 (6)

where τ is the integration time step for the time-fractional Smoluchowski solution, $n=t/\tau$ is the number of integration steps up to time t, $\Gamma(\cdot)$ is the Gamma function and $\omega_i^{(\alpha)}=j^{1-\alpha}-(j-1)^{1-\alpha}$.

Computational details

Molecular dynamics protocol

All the MD simulations reported in this study were performed using NAMD 2.12,⁴³ using the CHARMM36 force field for lipids⁴⁴ and the TIP3P water model.⁴⁵ A Langevin thermostat with a damping coefficient of 1 ps⁻¹ maintained the temperature at 308 K. The Langevin piston method⁴⁶ was used to maintain the system at a nominal pressure of 1 atm. Covalent bonds involving hydrogen atoms were constrained to their equilibrium length by the Rattle algorithm.⁴⁷ The Settle algorithm was utilized to constrain water molecules to their equilibrium geometry.⁴⁸ Long-range electrostatic forces were evaluated using the particle-mesh Ewald algorithm with a grid spacing of 1.2 Å while a smoothed 9-Å spherical cutoff was applied to truncate short-range van der Waals and electrostatic interactions. The r–RESPA multiple time-stepping algorithm was employed to integrate the equations of motion with an effective time step of 2 fs for short-range interaction and 4 fs long-range interactions.⁴⁹

Computational assays

The three permeants, ANA, DDA and HYL were used in the present investigation. ANA has a molecular weight of 222.2 g/mol, with a chemical structure of a tricyclic aromatic hydrocarbon. It is used in research as a chloride channel blocker. ^{50,51} DDA has a molecular weight of 235.2 g/mol, and is a dideoxynucleoside compound, in which the 3'-hydroxy group borne by the sugar moiety has been replaced by a hydrogen atom. It serves as an inhibitor of HIV replication and acts as

a chain-terminator of viral DNA by binding to the reverse transcriptase.⁵² HYL has a molecular weight of 362.466 g/mol, and is commonly used in the treatment of inflammation, allergy, and collagen diseases. Figure 1 depicts the chemical structures of these three permeants.

Figure 1: Structures of the three permeants studied in this work.

The force-field parameters for all three molecules were initially predicted, using the on-line CHARMM general force field (CGenFF) program (version 3.0.1). $^{53-55}$ For ANA and DDA, penalty values of the prediction were both zero. For HYL, charge penalty values up to 44.2 and dihedral penalty values up to 110 were reported. To assess the quality of the force field parameters, free-energy perturbation 56,57 (FEP) calculations were performed to determine the relative solvation energy of the three permeants in water and n-decane. The results of the simulations (Table S1) were then compared with the corresponding partition coefficients ($C_{\rm dw}$) measured experimentally . For the ease of comparison, $C_{\rm dw}$ was converted into a differential solvation free energy between the two environments, $\Delta\Delta G$, by $C_{\rm dw}=-\frac{\Delta\Delta G}{RT}$, where R is the molar Boltzmann constant and T is the temperature. Due to the uncertainty for HYL, three sets of force-field parameters were examined, namely those extracted from CGenFF, $^{53-55}$ those subsequently optimized via the FFTK plug-in 58 of VMD, 59 as well as those generated by the program GAMMP. Quite unexpectedly, the set of parameters obtained from the CGenFF server yielded the best agreement with the experimental reference, and was, therefore, utilized in our ABF calculations. It ought to be mentioned that although ANA shows a relatively large difference in the experimentally measured and compu-

tationally determined $\Delta\Delta G$, the final permeability value (see the Results section) shows no worse deviation from the experimental reference than the other two permeants. The hydrophobic nature of ANA dictates that the free-energy valleys within the lipid tail region contribute only marginally to the overall permeability, and, therefore, suboptimal force-field parameters do not appear to impact significantly the permeability estimate.

Two lipid bilayers were used in this work, namely a pure POPC bilayer and a POPC:cholesterol mixture at a 2:1 ratio. The initial bilayer patches were trimmed from larger membranes reported previously, 60 and subjected to a 100-ns equilibration. The equilibrated pure POPC bilayer consists of 64 molecules in each leaflet, while the sterol-rich models include 31 cholesterol and 62 POPC molecules in each leaflet. The bilayer model was therefore sufficiently large to accommodate undulations induced by penetration of ANA, DDA, and HYL, 61 which are relatively large permeants compared to those previously considered in simulation studies. The normal to the membrane coincides with the *z*-axis of Cartesian space. Each leaflet is in equilibrium with a layer of water at least 32 Å thick. The final computational assays had an area in the *x*, *y*-plane of about 67×67 Å², and a dimensions along the *z*-axis of 80–108 Å, and included 6,153–10,214 water molecules.

Steered MD simulations were performed to pull, in a near-equilibrium regime, each permeant through the membrane at a speed of 5 Å/ns, resulting a total simulation time of 100 ns. To enhance sampling efficiency, the reaction pathway was stratified in nine different windows, corresponding to initial positions of the permeant z = -35, -30, -20, -10, 0, +10, +20, +30, +35 Å. Each stratum was thoroughly equilibrated, restraining the position of the permeant to its center by means of a suitable harmonic potential. The thermalization time for the various windows is shown in Table S2.

Free-energy calculations

The ABF algorithm²² was used to determine the PMF, w(z), through integration of the average force exerted along the transition coordinate.^{21,62,63} The transition coordinate was defined as the projection onto the z-direction of Cartesian space, i.e., the normal to the membrane, of the distance

separating the center of mass of the permeant from that of the lipid bilayer. The total permeation pathway spans 90 Å, i.e., $-45 \le z \le 45$ Å. The pathway was broken down into nine strata, as listed above, each 10 to 15 Å wide and overlapping sequentially over 5 Å. In each stratum, the reaction pathway was discretized in bins 0.1 Å wide, in which samples of the local force acting along z were accumulated.²²

Kinetic modeling

The position-dependent fractional diffusivity, $K_{\alpha}(z)$, was determined using a variant of the Bayesianinference scheme developed for classical diffusion, ²⁹ and is implemented in the program DiffusionFusion. 30,31 For each of the nine strata and the six computational assays, we simultaneously optimized the fractional order, $\alpha(z)$, and the fractional diffusivity, $K_{\alpha}(z)$. The Bayesian-inference scheme was applied to the last half of the converged ABF trajectories, where the effective force on the permeant could be assumed to be zero. The fractional order $\alpha(z)$ reports how the apparent classical diffusivity varies with timescale; hence, to obtain convergence of $\alpha(z)$, it is helpful to consider displacements on different timescales. Therefore, we chose to partition the trajectory data into sets of displacements over lag times of $\Delta t=4$ and $\Delta t=16$ ps, with an equal number of displacement samples for each lag time. The functions $\alpha(z)$ and $K_{\alpha}(z)$ were represented with a grid spacing of 1 Å on a domain consistent with the given stratum. For each stratum/assay, optimization involved 5×10^5 Monte Carlo move attempts on randomly chosen grid points in $\alpha(z)$ and $K_{\alpha}(z)$. The Monte Carlo moves had long-tailed distributions ^{29,64} with characteristic scales of 0.005 in $\alpha(z)$ and 3.5 Å²/ns^{α} in $K_{\alpha}(z)$. Moves on both functions had acceptance ratios of 25-60%. The likelihood of the observed displacements was calculated by solving the fractional Smoluchowski equation (see equations 2 and 6) using an integration time step of $\tau=200$ fs. 30 The posterior probability appeared to converge after about 3×10^5 Monte Carlo steps; hence, the posterior distribution was generated from samples obtained after this threshold was reached. The mean and standard deviation of the posterior distribution determined the values of $\alpha(z)$ and $K_{\alpha}(z)$ and their uncertainties, respectively. The grids of $\alpha(z)$ and $K_{\alpha}(z)$ values on the full domain (i.e.,

-45 < z < +45 Å) were formed by joining the results of all strata and discarding points within 2 Å of their stratum boundaries.

The membrane permeability can be estimated by considering the net flux of substrate in the steady state, where the resistance against permeation can be expressed by introducing the position-dependent fractional diffusivity to equation 1,

$$R = \frac{1}{P_{\rm m}} = \int_{-\frac{L}{2}}^{\frac{L}{2}} dz \frac{\exp[\beta w(z)]}{K_{\alpha}(z)}$$
 (7)

Integration is performed over the thickness of the lipid bilayer, i.e., $-L/2 \le z \le +L/2$. The key difference between equation 1 and equation 7 lies in the replacement of D(z) by $K_{\alpha}(z)$, which represents two different physical pictures of motion within the membrane. Phenomenologically, the estimates of D(z) exhibit a strong dependence on the lag time, 30,31 whereas $K_{\alpha}(z)$ is independent of it. Lag-time dependence of the diffusivity is a hallmark of anomalous diffusion and underscores an inconsistency in the classical diffusion model to describe permeation events in lipid bilayers. To maximize the fidelity of the results, w(z) and $K_{\alpha}(z)$ were symmetrized about z=0 before the calculation of $P_{\rm m}$, weighted by the number of ABF samples for w(z) and the uncertainty of $K_{\alpha}(z)$ determined from its posterior distribution.

Void fraction and other analysis

Empty regions, or voids, within the simulation cell were identified by mapping atomic configurations from the MD trajectories onto a three-dimensional grid with a uniform spacing of approximately 0.5 Å. Each non-hydrogen atom was considered as a sphere with a radius equal to $R_{\rm min}/2$ as defined in the CHARMM36 force field, ⁵³ plus an additional probe radius of 1.5 Å. All voxels of the grid were marked as either being occupied by an atom or empty, using a cell-decomposition algorithm. The empty grid voxels were then subjected to a flood-fill algorithm to identify contiguous voids. For the purpose of the flood fill, two grid voxels were considered to be connected if they shared any vertex, i.e., each voxel had 26 neighbors. Additional detail on the void-identification

analysis can be found in reference 30.

Analysis of the permeant orientation, the dipole moment, the number of surrounding water molecules, as well as the distribution of lipid height, the cholesterol orientation, the pair-correlation functions, or g(r), and the number of flip-flop events were performed using VMD. More specifically, the calculation of cholesterol flip-flop events was performed for each of the nine strata separately, i.e., flip-flop events at a given window were determined separately and the numbers from all windows were then summed up. For the calculation of the void density and the magnitude of the dipole moments, the data from the two leaflets were symmetrized.

Results

Translocation free energy of the permeant across the membrane

Using the ABF algorithm, 22 we determined the free-energy profile underlying permeation of ANA, DDA, and HYL through a pure POPC bilayer and a bilayer formed by a POPC:cholesterol (2:1) mixture. The simulation time for each system is shown in Table 1 and spans the multi- μ s timescale — roughly 2–5 μ s. While our simulations were performed over the entire translocation pathway, i.e., $-45 \le z \le +45$ Å, given that the two leaflets in our bilayers are identical, the free-energy profiles can be symmetrized a posteriori — a prerequisite for the determination of $P_{\rm m}$ from equation 7. The symmetrized PMFs obtained by anti-symmetrizing the gradients, are shown in Figure 2. It ought to be mentioned that the symmetrized and non-symmetrized PMFs may be compared as an indicator of the convergence of the free-energy calculations, i.e., in the hypothetical limit of infinite sampling, the asymmetry in w(z) with respect to z=0 should vanish. The error bars associated to the graphs of Figure 2 reflect the deviation from an ideal, symmetric free-energy profile. Our simulations were pursued until the asymmetry between the upper and the lower leaflet, or the hysteresis in the free energy between z=-45 and z=+45 Å was less than $k_{\rm B}T$, thereby, rationalizing the substantial amount of sampling invested for each permeant.

As a hydrophobic permeant, ANA yields a negative w(z) throughout the membrane with a free-

energy minimum about 6.5 kcal/mol deep, below the aqueous interface, on both sides of the lipid bilayer, and a barrier peaked at its geometric center, z=0. In stark contrast, for the hydrophilic permeant DDA, a large free-energy barrier is found at the center of the bilayer, culminating at about 7.5 kcal/mol. HYL represents an intermediate case between ANA and DDA, featuring a free-energy minimum about 3 kcal/mol deep, located below the aqueous interface, and a barrier centered at z=0, about 3 kcal/mol high. Interestingly enough, both the PMF of DDA and that of HYL exhibit a small, secondary free-energy barrier found in the vicinity of the lipid head-group region. A summary of the free-energy values at z=0, for the three permanents, is shown in Table 1.

In the analysis presented in the following section, we focus on two regions of the PMFs for each permeant, namely the *peak* region within the membrane, defined as a 10-Å window centered at z=0, and the *valley* regions, defined as two 10-Å intervals centered at the PMF minima within the membrane, , $z=\pm 10$ Å for ANA (POPC), $z=\pm 14$ Å for DDA (POPC), $z=\pm 11$ Å for HYL (POPC), $z=\pm 13$ Å for ANA (POPC:cholesterol), and $z=\pm 14$ Å for HYL (POPC:cholesterol). While the PMF of DDA in POPC:cholesterol does not have any valley, the location of a small dip in the PMF ($z=\pm 20$ Å) is chosen for comparison purpose. Representative snapshots at these regions from ABF simulations of the three permeants are shown in Figure 3.

Table 1: Simulation times of the ABF calculations and the free energy at bilayer center.

Permeant	Bilayer	Simulation time (μ s)	w(z) at $z=0$ (kcal/mol)
ANA	POPC	5.376	-2.59 ± 0.83
ANA	POPC:cholesterol	2.700	-2.61 ± 0.43
DDA	POPC	2.122	7.52 ± 0.15
DDA	POPC:cholesterol	2.467	8.28 ± 0.47
HYL	POPC	2.605	3.44 ± 0.56
HYL	POPC:cholesterol	3.600	6.25 ± 0.60
Aggregate time (µ	us)	18.870	

Comparison of the free-energy profiles obtained in the POPC:cholesterol mixture with those characteristic of the pure POPC environment reveals a remarkably similar shape and free-energy differences for both ANA and DDA. Conversely, for HYL, the PMFs show similarities in the

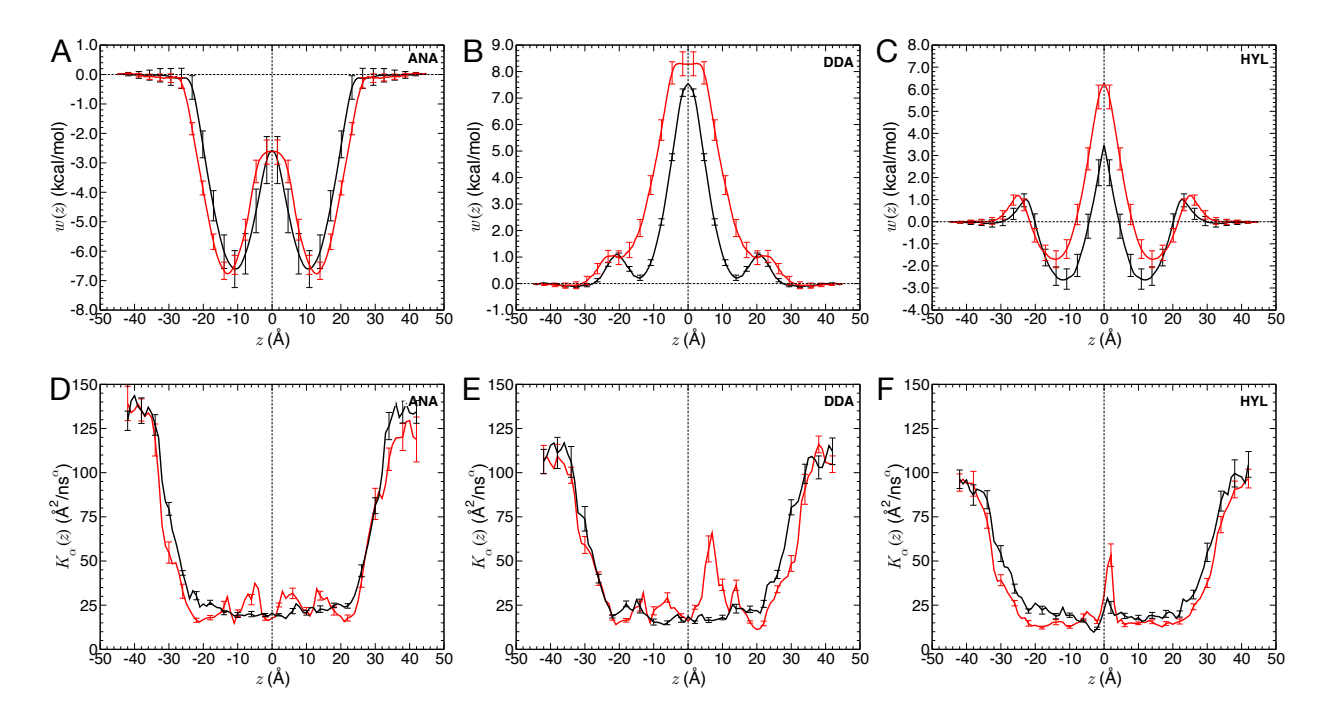


Figure 2: Free-energy profiles w(z) and positional dependent fractional diffusivities $K_{\alpha}(z)$ for permeation of ANA (A, D), DDA (B, E) and HYL (C, F) in pure POPC (black) and POPC:cholesterol mixture (red). The coordinate z is the distance between the center of lipid bilayer and the COM of the permanents. The error bars represent the estimated uncertainty of the free-energy and diffusivity for moving the permanents.

shape, but with a near 80% increase of the free-energy barrier at the center of bilayer (see Table 1). This significant numerical difference appears to arise from the unique interactions of HYL with the membrane, as will be discussed further in the next sections. For all three permeants, a broadening of the free-energy profile, both in the valleys and in the barrier regions, is observed. Such a broadening reflects the well-known effect of cholesterol in condensing and ordering lipid bilayers, 37,38,65 resulting in an increased thickness of the POPC:cholesterol mixture, relative to the pure POPC membrane (see Figure S1). Indeed, we find that the cholesterol-rich bilayer is about 6 Å thicker than the pure POPC bilayer — specifically the average distance between the phosphorus atoms of the two leaflets is 37.9 ± 0.6 Å (mean \pm SD) for the pure POPC system and 43.7 ± 0.5 Å for the POPC:cholesterol system. In the particular case of DDA, the broadening due to the presence of cholesterol caused the local minima below the aqueous interface to disappear in the POPC:cholesterol mixture.

Fractional diffusivity of the permeant across the membrane

The position-dependent fractional-diffusivity profiles, $K_{\alpha}(z)$, for the different permeants in pure POPC and in the POPC:cholesterol mixture are shown in Figure 2. The three profiles obtained in the pure POPC simulations exhibit very similar features, with the bulkier amphiphilic HYL possessing the lowest fractional diffusivity. Interestingly, the introduction of cholesterol does not significantly impact the fractional diffusivity, except that the region of low $K_{\alpha}(z)$ is slightly broader, consistent with greater thickness of the membrane as noted above. However, a conspicuous bump in $K_{\alpha}(z)$ is observed in the vicinity of z=0 for HYL and DDA. As will be discussed later in the text, this surge of the fractional diffusivity is consistent with a greater density of voids near the center of the bilayer. We have previously emphasized that such empty spaces are critical for the long, albeit rare jumps of the permeant amid the lipid chains. The values of $K_{\alpha}(z)$ far from the membrane (i.e., |z| > 35 Å) are consistent with independent simulations to measure the classical diffusivity of the compounds in a box of water. Using the Einstein–Smoluchowski formula, $D = \lim_{t \to \infty} \left\langle [\mathbf{r}(t) - \mathbf{r}(0)]^2 \right\rangle / 6t$, we found bulk diffusivities of 127 ± 3 , 98 ± 2 , and 82 ± 2 Å²/ns for

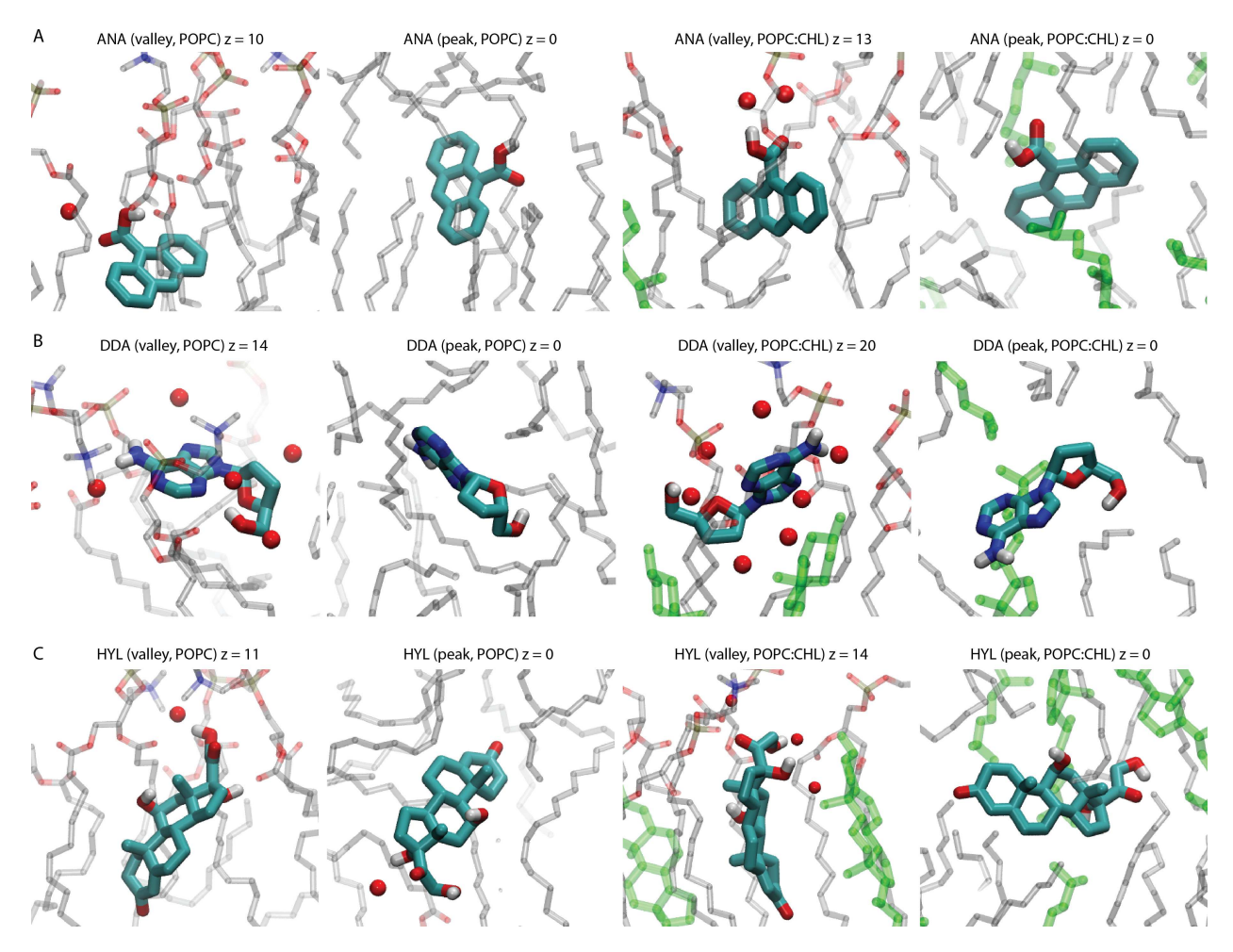


Figure 3: Snapshots of ANA (A), DDA (B) and HYL (C) in the peak and valley regions of their PMFs in POPC or POPC:cholesterol (POPC:CHL) membranes. Cholesterols are colored in green, and water molecules within 2.4 Å of the permeants are shown as red spheres. See Results for the definitions of peak and valley regions for each permeant.

Membrane permeability to the permeant

The membrane permeability, $P_{\rm m}$, to the three permeants was calculated using the aforementioned PMFs and the fractional-diffusivity profiles, and is reported in Table 2, together with the values measured experimentally using egg lecithin/n-decane membranes.⁸

Table 2: Calculated permeability values of each permeant in pure POPC and POPC:cholesterol. *Experimental values 8 obtained with an egg lecithin membrane are also included.

Permeant	Environment	$P_{\mathrm{m}} (\mathrm{cm} \mathrm{s}^{-1})$
ANA	Egg lecithin*	3.2 ± 0.8
ANA	POPC	20.1 ± 0.1
ANA	POPC:cholesterol	24.4 ± 0.2
HYL	Egg lecithin*	$(5.6 \pm 0.3) \times 10^{-4}$
HYL	POPC	$(4.2 \pm 0.5) \times 10^{-1}$
HYL	POPC:cholesterol	$(7.0 \pm 2.0) \times 10^{-4}$
DDA	Egg lecithin*	$(6.3 \pm 0.1) \times 10^{-5}$
DDA	POPC	$(2.0 \pm 0.2) \times 10^{-4}$
DDA	POPC:cholesterol	$(2.8 \pm 0.5) \times 10^{-5}$

Strikingly, all the permeabilities derived from the simulations are within one order of magnitude from the experimental value measured in egg lechithin/n-decane membranes, with the exception of the permeability value of HYL calculated using the pure POPC bilayer model. This outlier is more than three orders of magnitude higher than the experimental egg-lecithin value and, intriguingly, our own estimate in the POPC:cholesterol membrane. This apparent high sensitivity of the HYL permeability to the membrane composition is analyzed further below. The remaining numerical discrepancies between experiment and simulation can likely be attributed to the difference in the membrane compositions between the models and the egg lecithin/n-decane membrane and/or imperfections in the pairwise additive force field used herein. To the best of our knowledge, this is the first permeability calculation involving these three molecules. Considering, on the one hand, the incertitude on the experimental assay, notably the membrane composition, and, on the other hand, the likelihood of large systematic error burdening our free-energy calculations, the

present results are rather encouraging.

The composition of the egg-lecithin/n-decane membrane employed in the experiments⁸ is somewhat complex and cannot be readily compared to either of the computational assays. However, pure POPC should serve as a crude model of egg lecithin, because phosphatidylcholine represents about 80% of the lipids therein, and the most common alkyl tails for these lipids are the same as those in POPC, i.e., palmitic acid (16:0) and oleic acid (18:1). 66 Other components include, among others, phosphatidylethanolamine, lysophosphatidylcholine and sphingomyelin. One study ⁶⁶ reported that egg lecithin produced on a large scale has a remaining cholesterol amount of about 2% by weight, that is, approximately 4% by molar fraction. Thus, although cholesterol is likely present in egg lecithin/n-decane membranes, its concentration is lower than in our POPC:cholesterol bilayer model. On the other hand, the egg lecithin/n-decane membranes contain non-negligible concentrations of 20-carbon lipid tails and phosphoethanolamine head groups, ⁶⁶ which altogether likely increase the thickness of the egg lecithin/n-decane membrane, relative to that of pure POPC. 67 The egg lecithin/n-decane membrane, just like our computational model of a POPC:cholesterol bilayer, is a few angstroms thicker than a pure POPC bilayer. Consistent with this observation, the calculated permeability of HYL in our thicker POPC:cholesterol bilayer is within statistical uncertainty of the experimental value, while the calculated permeability in pure POPC disagrees by several orders of magnitude. Still, it remains unclear whether the pure POPC or POPC:cholesterol model should be considered as a better approximation of egg lecithin/n-decane.

It is interesting that neither the permeability of DDA nor that of ANA is strongly affected by the change of model from pure POPC to POPC:cholesterol, which might be explained by the fact that HYL is considerably bulkier than DDA and ANA. As will be discussed at length in the next section, of all three permeants, HYL exhibits the highest sensitivity to a change in its environment, notably from pure POPC to a POPC:cholesterol mixture. This sensitivity is related to the non-local perturbation induced by the permeant within the bilayer, which, in turn, may render the molecule particularly susceptible to structural heterogeneity of the membrane. Therefore, compared with the pure-POPC bilayer used in our simulations, it is conceivable that a different response may

be expected from HYL to the egg lecithin/n—decane membrane used in experiment, which could correspond to a higher free-energy barrier against HYL permeation. In stark contrast, the difference in the response induced by the surroundings is unlikely to be significant for ANA and DDA, given the highly localized perturbation the two permeants generate in the bilayer. The lesser sensitivity to a heterogeneous lipid environment is, indeed, manifested in the similar membrane permeability in pure POPC and in a POPC:cholesterol mixture. The role played by these different factors will be examined in further detail in the following section.

It should also be noted that the permeabilities calculated for ANA in Table 2 are more ambiguous than for the other two permeants on account of its lipophilic nature. In These limits of integration are somewhat arbitrary owing to the fact that membrane surface fluctuates and is not well defined at the atomic level. The integrand in equation 7 can be thought of as a permeation resistance density that increases exponentially with increasing free energy, and is inversely proportional to the local diffusivity. In the cases of HYL and especially DDA, any reasonable choice of the limits of integration will give effectively identical values since the integral is dominated by regions of large free energy near the center of the membrane (|z| < 10 Å). On the other hand, ANA is sufficiently lipophilic that the free energy within the bilayer is lower or similar to the value in the aqueous solution at all points (Figure 2A). However, the slower diffusion of ANA near and within the membrane, relative to the aqueous solution (Figure 2D), ensures that the permeation resistance density of the membrane is greater than that in water. As shown in Figure S2, the maximum permeation resistance density for ANA occurs at the water--head-group interface ($z \sim 24.1 \text{ Å}$ in pure POPC and $z\sim 26.5$ Å in the POPC:cholesterol mixture), whereas it occurs near z=0 for HYL and DDA. Furthermore, it can be seen that the integral in equation 7 can depend significantly on the choice of the integration limits. In effect, the permeability of ANA is not well defined, and there should be a certain arbitrariness in the value determined by experiment as well. Moreover, in the simulations, the free energy and kinetics are determined using models containing only one single permeant. The concentrations of drug-like molecules are usually quite low in experiments (for example ⁶⁸ < 1 mmol/L), as well as in clinical applications of drugs, making these models a

good approximation of the reality under most circumstances. In the case of ANA, however, the free-energy minimum within the membrane is -6.62 ± 0.11 and -6.78 ± 0.05 kcal/mol for the pure POPC and the sterol-rich assays, respectively, making the ANA occupancy within the bilayer relativity high, even for dilute aqueous concentrations. The areal density at equilibrium within one leaflet can be estimated as $S = C_0 \int_0^{L/2} \mathrm{d}z \, \exp{[-\beta w(z)]}$. Thus, for an aqueous concentration of $C_0 = 100 \, \mu \mathrm{mol/L}$, the areal density of ANA molecules in a single leaflet would be $\sim 2 \, \mathrm{mm}^{-2}$, likely sufficient to perturb the structure of the membrane (see Figure S1) and affect permeation of the ANA molecules themselves. In summary, numerical values of the permeability for highly lipophilic permeants such as ANA are particularly sensitive to the method of calculation and to the experimental protocol, and can, moreover, be conceptually ill-defined.

Differential impact of cholesterol on permeant translocation

The membrane permeability of all three permeants in the POPC:cholesterol mixture is consistently lower than that in pure POPC, in line with previous theoretical investigations of solute partitioning in sterol-rich lipid bilayers. ³⁸ As noted previously, cholesterol exerts a significantly different influence on the reversible work incurred by the three permeants to traverse the membrane. Specifically, the PMF of HYL in the POPC:cholesterol mixture has an approximately 3–kcal/mol higher peak at the bilayer center (i.e., 80% of the nominal value), whereas only a 10% increase is observed for both ANA and DDA. In this section, we associate the physical origin of the above observation with the differential influence of cholesterol on the interaction of the three permeants with the bilayers. In a nutshell, our analysis indicates that, on the one hand, HYL responds to its lipid environment differently from ANA and DDA, as manifested by the pronounced anisotropy of its orientation and dipole moment within the membrane as well as its reduced level of hydration. On the other hand, our analysis also reveals how HYL generates a significantly larger perturbation to the lipid environment, especially in the sterol-rich membrane, which extends to distances never observed for ANA, DDA or, to the best of our knowledge, most other small compounds reported in the literature.

Figure S3 depicts the average orientation of the three permeants along the membrane normal

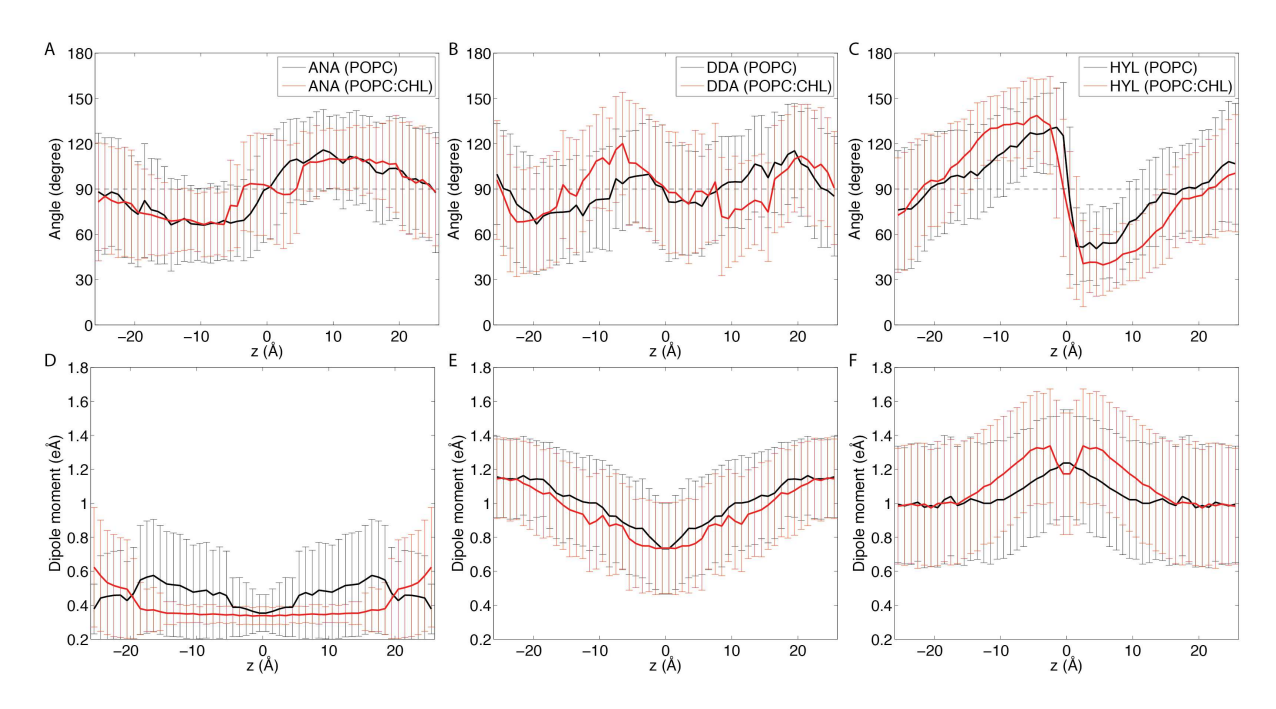


Figure 4: Orientation and magnitude of the dipole moments of the three permeants as a function of their COM (z). Dipole orientation (A–C) is measured as the angle between the dipole vector and the z axis, while the magnitude of the dipole moment, symmetrized over the two leaflets, is shown in D-F. Error bars depict standard deviations.

in pure POPC and in the sterol-rich medium, together with the set of atoms used to define the orientation. Figure S3 reflects the hydrophilic and hydrophobic moieties of each permeant are organized spatially during membrane permeation, where an angle less than 90° in the upper region (z>0) and greater than 90° in the lower region (z<0) indicates that the hydrophilic group points towards water. Comparison of the three permeants reveals that whereas all of them have an antisymmetric profile and flip their orientations at the bilayer center, such flip is particularly abrupt for HYL. In pure POPC, its orientation switches from \sim 150° at z=-3 Å to \sim 30° at z=3 Å, indicating that the molecule undergoes a dramatic reorientation over a narrow region at the bilayer center. A similar behavior is observed in the POPC:cholesterol mixture, with a slight broadening of the region across which the flip occurs, i.e., from z=-5 to z=5 Å. In contrast with HYL, both ANA and DDA undergo smoother reorientations. The smaller sizes of the latter two permeants, and in the case of DDA, the rotational freedom of the adenosine moiety relative to the deoxyribose ring, may have contributed to a more isotropic orientation within the membrane.

It is worth mentioning that no antisymmetric orientation profile is observed for ANA and DDA if a different set of atoms is used to define their orientation (see Figure S3).

The distinct response of the three permeants to their lipid environment is further demonstrated by the change in their dipole moment across the membrane. As a reference, the electrostatic potential of the pure POPC bilayer and POPC:cholesterol mixture determined via the PMEPOT plug-in⁶⁹ of VMD is shown in Figure S4. The positive electrostatic potential at the bilayer center, consistent with the results of previous theoretical investigations, 70 dictates that a dipole moment aligned with the membrane electrostatic field, i.e., an angle less than 90° in the upper region and greater than 90° in the lower region, is energetically favorable. As shown in Figure 4, only the dipole moment of HYL is aligned parallel to the electric field. The alignment is far less optimal with DDA and for ANA, the alignment is antiparallel. Furthermore, the magnitude of the dipole moment of HYL increases within the membrane, whereas a decrease is observed in DDA and ANA. This behavior can be explained by the different chemical structures of the permeants and their orientation within the membrane. For ANA, the dipole moment is dictated by the carboxyl moiety. Since the latter is expected to point towards water, the dipole moment is aligned antiparallel with the electric field (see Figure 3 A). Rotation of the hydroxyl group and anthracene ring may reduce, but not fully resolve the antiparallel alignment. Similarly, the hydroxyl group of DDA is oriented towards water, although the rotational freedom of its adenosine group relative to the deoxyribose ring confers to the molecule a greater flexibility to align its dipole moment parallel to the membrane electrostatic field. Interestingly, when such an alignment cannot be fully achieved, ANA and DDA appear to adopt a different strategy, namely, to reduce the magnitude of their dipole moment (see Figure 4 D, E) through isomerization. As noted above, the latter is achieved through rotation of the hydroxyl moiety in ANA, and rotation of both the hydroxyl moiety and the deoxyribose ring relative to the adenosine group in DDA. In contrast to ANA and DDA, an aligned dipole moment is not antinomic with the requirement that the hydrophilic group of HYL be oriented towards water. Indeed, HYL appears to maximize its favorable electrostatic interactions with the membrane by increasing the magnitude of its dipole moment through the rotation of its three hydroxyl groups

(see Figure 3 C).

Translocation of a permeant across lipid membranes has been long known to be frequently accompanied by a retinue of water molecules ensuring proper hydration. Figure S5 shows the number of water molecules within the immediate vicinity (2.4 Å) of the three permanents. As expected, the hydrophilic DDA and HYL attract more water than ANA, although the larger size of the former two permeants may also play a role. Unlike DDA, HYL has a nonzero number of surrounding water molecules, even at the center of the bilayer, indicating that it is capable of preserving, at least in part, its hydration shell deep into the hydrophobic core. This discrepant property contributes to the significantly smaller free-energy barrier of the latter molecule in POPC (Table 2). In stark contrast with pure POPC, HYL relinquished nearly all of its hydration water molecules at the center of the POPC:cholesterol mixture, reflecting the increased rigidity and thickness of the latter membrane. The differential hydration profiles of the permeants may explain, at least in part, the much greater sensitivity of HYL towards the presence of cholesterol in a phospholipid membrane.

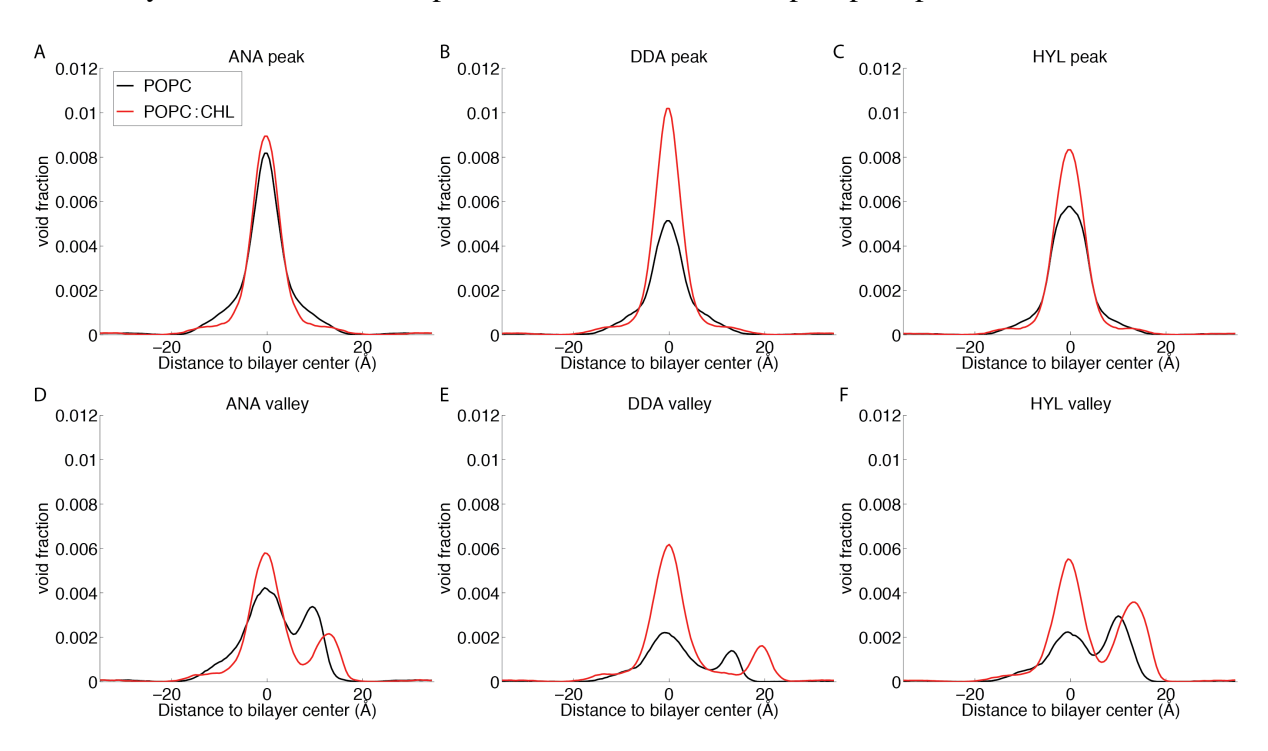


Figure 5: Void density profiles in pure POPC (black) and POPC:cholesterol (red) with the permeants at the peak (A-C) and in the valley regions (D-F) defined in the Results section. Data from the two leaflets were symmetrized and presented in D-F as if the permeant were located in the valley region within the upper leaflet (z > 0).

As described in the previous section, the fractional order for the three permeants is less than 1.0, in both the POPC and POPC:cholesterol assays, thereby indicating that their translocation across the membrane is subdiffusive. The origin of such a subdiffusive behavior may be due to the formation of a number of discrete, low-density regions, or voids within the lipid bilayer, which undergo dynamics on relatively long timescales (many picoseconds), and are typically much larger than voids that appear spontaneously in water. 30 These voids are identified algorithmically, as described in the Methods section. Figure 5 shows the void density of the POPC and POPC:cholesterol assays, with the permeants either at the peak or in the valley regions defined previously. It ought to be noted that the volume of the permeants themselves is also counted towards the void. As expected, the voids occupy only a small fraction of the total space, and are substantial in number at the center of the bilayer, in line with the findings of previous studies. ^{19,30,71} When the permeants reside in bulk water, the void fraction at the center of all bilayer assays fall within the range of 2-3% (data not shown), which can be viewed as the void fraction spontaneously formed within the membrane, i.e., in the absence of the permeants. Interestingly, the void fraction is significantly increased at the bilayer center even before the permeants reached this location (see Figure 5), supporting that void formation precedes the permeation event itself. In pure POPC, such an increase is particularly evident for ANA, which can be explained, at least in part, by the close proximity of its valley region ($z = \pm 10\text{Å}$) to the bilayer center. In all POPC:cholesterol assays, such an increase of the void fraction caused by the permeants is much more significant than in the corresponding pure POPC assays, consistent with the rigidifying effect of cholesterol, which confers to the structural perturbation a more nonlocal character.

The comparison between void fraction in the pure-POPC and POPC:cholesterol assays provides additional insight into the subdiffusive nature of the translocation of the three permeants. For HYL and DDA, the void fraction shows a significant increase at the center of the POPC:cholesterol bilayer, compared to pure POPC (60% for HYL, 100% for DDA), while it remains similar for ANA. Making a parallel between this result and the fractional diffusivities presented in the previous section, one observes a positive correlation between $K_{\alpha}(z)$ and the void density at the center

of the bilayer, again supporting the notion that the movement of the permeant is facilitated by the formation of voids, driven by subdiffusive lipid motion on the 1 ps to 10 ns timescale.⁷²

In order to investigate thoroughly the perturbation induced by the three permeants onto bilayer structure, we further analyzed the height of the POPC molecules, as well as the orientation of cholesterol in the mixed bilayer. With the bilayer center located at z=0, Figure S1 depicts the height of the lipid molecules, measured as the z coordinate of the phosphorus atoms in POPC or the hydroxyl oxygen atom in cholesterol, as a function of their distances to the COM of the permeant. Only the statistics collected with the permeant lying either at the peak or in the valley regions defined previously were used in the analysis. For pure POPC, DDA and HYL induce a more pronounced decrease in the lipid height at the peak of the PMFs, i.e., ~4 Å for lipids immediately surrounding DDA and HYL, and ~3 Å for ANA. It is worth noting that the lipid height distribution did not plateau until $r \sim 30$ Å, reflecting the long-range nature of the structural perturbation induced by the permeants. Similar observations are made with the POPC:cholesterol assay, although the impact of ANA and DDA is now both considerably weaker than HYL. Overall, the above results again reflect the differential impact of cholesterol on the three permeants — while pure POPC readily "absorbs" the perturbation through adjusting the lipid height and tail order (data not shown), the sterol-rich membrane is far less accommodating, with the long-range structural changes suppressed for both ANA and DDA. Only the bulkiest HYL could introduce a relatively large ($\sim 4\,\text{Å}$) and far-reaching ($r \sim 30\,\text{Å}$) decrease in the height of POPC and cholesterol. A similar trend is observed in the analysis of the cholesterol orientation around the three permeants (Figure S6). While considerable tilting of the cholesterol molecules is found within the immediate vicinity of all three permeants residing near the peak of their PMF, tilting is again far-reaching $(r \sim 30 \, \text{Å})$ only in the case of HYL. Furthermore, cholesterol from the opposite leaflet appears to be also influenced by the presence of HYL, which was not observed with either ANA or DDA.

The lipid-height and cholesterol-orientation profiles of HYL both bring to light an oscillation pattern not found with either ANA or DDA. In essence, this pattern arises from the distribution of the cholesterol molecules within a POPC:cholesterol mixture — previous lipid mixing simula-

tions⁶⁰ have revealed such a signature oscillation pattern in the two-dimensional radial pair distribution function, or g(r), of cholesterol molecules. For a permeant with an overly rigid scaffold and fixed orientation within the membrane, e.g., HYL, the same oscillation pattern will be manifested in the g(r) between the permeant and the sterol (see Figure S7). In contrast, for a relatively flexible permeant, e.g., DDA, or for a permeant with a more isotropic orientation within the membrane, e.g., ANA, the oscillation is considerably damped. These differences provide a structural basis for HYL to exert its relatively long-range perturbation to the lipid bilayer. As an illustration, a snapshot from the HYL (POPC:cholesterol) simulation is shown in Figure S8, where it can be seen that the molecular tilt introduced by the permeant can readily propagate from one sterol to another.

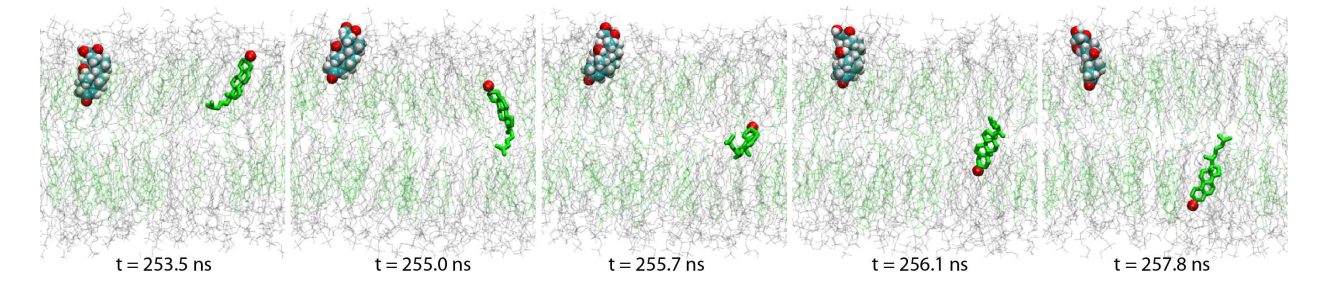


Figure 6: Cholesterol flip-flop observed during ABF window 3 simulation of HYL.

Interestingly enough, our analysis also reveals an increased flip-flop rate in some of the bilayers. Specifically, no flip-flop event was witnessed in the pure-POPC simulations. In the POPC:cholesterol mixture of all three permeants, flip-flop of the cholesterol molecule $^{73-75}$ was, however observed — two events were recorded throughout the 2.7- μ s ANA simulations, while four and eight events were recorded for DDA ($2.5~\mu$ s) and HYL ($3.6~\mu$ s), respectively. A typical flip-flop event is shown in Figure 6. It is noteworthy that the cholesterol flip-flop needs not occur within the immediate vicinity of the permeant. Instead, as shown in Figure 6, the flipped cholesterol molecule can be rather distant from the permeant, again indicating that the perturbation caused by HYL is nonlocal. It is clear from the above result that the larger HYL generates considerably more flip-flop events than either ANA or DDA, even taking into account the different lengths of the simulations. This result correlates well with the increased tilt of cholesterol in the HYL (POPC:cholesterol) simulations (see Figure S6), since flip-flop of cholesterol must be prefaced by its reorientation. This

finding resonates with the message from the rest of our analysis, i.e., the bulky HYL generates a considerably larger perturbation to the bilayer than both ANA and DDA.

For completeness, we should add that our analysis of a previous 2- μ s Anton trajectory of a POPC:cholesterol mixture ⁶⁰ did not reveal any flip-flop event. While the difference in simulation settings may have contributed to the increased flip-flop rate observed in the present simulations, the relative comparison of the three permeants should not be affected. Moreover, the area per lipid determined from our pure POPC assays is approximately 69.3 Å² when the permeants are in bulk water, which compares favorably with the experimental reference of 68.3 ± 1.5 Å². ⁷⁶

Given the structural similarity between HYL and cholesterol, it is interesting to compare the movement of the two molecules across the membrane. As shown in Figure 6, the flip-flop event, once it happens, proceeds extremely fast. Even though our ABF calculation does not portray a complete permeation event of HYL in a single window, the orientation analysis performed over all windows clearly reveals flip flop-like motion, i.e., the HYL molecule prefers to expose its two terminal hydroxyl moieties to water, thereby, switching its orientation by 180° when crossing the center of the bilayer. Furthermore, similar to cholesterol, HYL can reside favorably within the lipid tail region, as supported by the energy valley in Figure 2. This feature clearly distinguishes HYL from ANA and DDA, i.e., the membrane constitutes both a sink and a barrier for the former permeant, but is exclusively a sink or a barrier for the latter two permeants. This difference has key implications in the nature of the membrane perturbation induced by the permeants — while all three compounds can induce considerable structural perturbation to the membrane when they reach z=0, such a perturbation is bound to be transient due to the fleeting nature of barrier-crossing events. Nonetheless, HYL is capable of exerting a significant influence on cholesterol orientation (see Figure S6) even when it resides in the lipid-tail region. Together with the increased cholesterol flip-flop rate in the HYL simulations, this result hints at possible cooperative permeation, i.e., when multiple HYL molecules are present in the membrane, bilayer structural perturbation induced by one HYL may help accelerate the flip-flop of the others. Such a scenario, which will only become relevant when local concentration of the permeant exceeds a certain threshold, remains to be further

investigated in future studies.

Conclusion

Here, we have analyzed the permeability of a pure phospholipid bilayer and a cholesterol-rich phospholipid bilayer to three biologically active permeant compounds. These permeants cover a wide range of physicochemical properties typical of drugs, with masses from 222 (ANA) to 362 Da (HYL), and n-decane-water partition coefficients from 3.6×10^{-6} (DDA) to 1.2 (ANA). Their experimentally determined permeability through an egg lecithin bilayer spans more than four orders of magnitude. With the exception of HYL in pure POPC, all of the calculated permeabilities fall within an order of magnitude of the experimental permeability values for the same permeant. 8

Order-of-magnitude agreement between experiment and theoretical predictions is generally sufficient for many applications, and probably the best that can be expected today, owing to several factors. First, the composition of the membrane and, presumably, its structure, differs between the experiments and the simulations. At first sight, the permeabilities calculated using the pure POPC model might be more directly comparable to those measured experimentally using an egg lecithin/n-decane membrane. ⁶⁶ However, despite the chemical similarity between a pure POPC bilayer and the egg lecithin/n-decane membrane, we expect the latter to be slightly thicker due to the inclusion of 20-carbon lipid tails and phosphoethanolamine head groups. ⁶⁷ Suggestively, the calculated permeabilities using the thicker POPC:cholesterol bilayer agree better with the experimental values for HYL and DDA (within a factor of three), while for ANA the level of agreement is similar. It would be interesting to construct a more realistic model of the egg lecithin/n-decane membrane to assess whether such a model yields a better agreement with the egg-lecithin experimental permeabilities. However, if our primary goal is to predict permeation through human intestinal epithelia, an alternate model might be more appropriate.

Like molecular simulations, experiments aimed at determining the permeability of drugs make use of model assays intended to represent absorption of orally administered drugs. Popular models

include PAMPA, based on artificial membranes, or those based on cell cultures, such as Caco-2 and the low-efflux MDCK and its RRCK variants. Similar to the computational approach presented here, PAMPA models do not consider possible active transport mechanisms or other possible influence of membrane proteins on drug transport; they, however, often attain high correlation with more complex cell culture models, such as Caco-2 and MDCK. There is little agreement about which of these methods gives the optimal balance between reliable prediction and costeffectiveness. Quantitative Structure–activity relationships (QSARs), which are calibrated based on experimental data, are another computational tool for predicting membrane permeability to drugs. While their computational cost is much lower than the molecular simulations presented here, they are reliant on a suitable training set and can become unreliable for permeants with substantially different properties than those in the training set or under sufficiently different conditions. 14 For example, QSARs trained for a particular membrane model and composition likely need to be retrained if predictions for a different type of membrane are desired. Because they are based on physical principles, molecular simulations can yield reliable predictions for a diverse range of permeant chemistries under a wide range of different conditions, and could even serve as a convenient means to train QSAR models, or to provide a reference for membrane-permeability calculations based on coarse-grained simulations. 77 It seems clear that molecular simulations complement other methods by revealing the physical phenomena underlying the process of permeation, and how it might be affected by the membrane composition.

Another possible source for the remaining discrepancies between the permeabilities derived from experiment and theory are imperfections in the intermolecular interaction potentials, or force field used in the simulations. As shown in Table S1 of the SI, differences in the method used to obtain atomic partial charges and bonded parameters and calculated permeability. This change of HYL behaviors with different approaches to the parameterization further underscores that the membrane permeability to HYL is particularly sensitive to the atomic detail. If the most important contribution of MD is to reveal the atomic-scale physical effects that underlie membrane permeability, then the semiquantitative accuracy of existing force fields may be sufficient. Force fields

that include atomic polarizability promise more physically accurate depictions of the transfer from nonpolar to polar phases, and might, thus, lead to more accurate predictions of the permeability at the price of an increased computational cost. Clearly, many-body induction effects may modulate the membrane dipole potential, which, in turn, can impact permeation events. Ralthough coverage of the chemical space by polarizable force fields is growing (for instance, POPC has recently been parameterized for the CHARMM Drude force field Physical parameterization of many drug-like molecules and chemical groups remains unavailable. Although our subdiffusive model appears to represent the motion of permeants in the bilayer better than the popular classical model, the may also have limitations in its own right. Moreover, this model can only assimilate phenomena that are observed in the simulation. Large molecular rearrangements, including lipid flip-flop, which was observed occasionally for HYL, may not be well sampled in simulations amounting to just a few microseconds.

Discrepancies between experiment and theory have, in some cases, been attributed to how the former has been interpreted. Reference and simulations is particularly subtle for lipophilic molecules like ANA, lacking substantial free-energy barriers to permeation, and for which the calculation of the permeability from both experiment and theory depends on the how the boundary of the membrane is defined. Furthermore, for lipophilic permeants, the bilayer acts as a trap, accumulating a density of permeants sufficient for substantial permeant—permeant interactions, even at aqueous concentrations that might be naively considered dilute ($\sim 100 \mu$ mol/L), making the effective permeability observed in experiments sensitive to the permeant concentration. Furthermore, the assumptions used in deriving the permeability from experimentally measured quantities may break down for such compounds. Reference and simulations is particularly subtle for lipophilic permeants, and the original subtle for lipophilic permeants are permeant interactions.

Our simulations predict a 600-fold decrease in the permeability of HYL between the pure POPC bilayer and the POPC:cholesterol bilayer (2:1 mole ratio). Meanwhile, the effect of cholesterol on the permeabilities of ANA and DDA is less than 50%. It seems plausible that the sensitivity of the permeability of HYL to the presence of cholesterol in the bilayer is linked to the fact that this compound induces longer range perturbations of the membrane structure than either DDA or

ANA. It remains unknown whether the large decrease in the permeability of the membrane to HYL when cholesterol is added to the membrane is a direct result of the interaction of the compound with cholesterol, or an indirect of effect caused by cholesterol altering the overall structure of the membrane, e.g., its thickness. Stated differently, our simulations suggest that HYL exhibits a permeation rate selective for the pure POPC bilayer over the POPC:cholesterol by a factor of 600. The possibility of such a significant selectivity suggests that a molecule might be designed for high permeability through membranes of a particular composition and structure, while maintaining a low permeability for other membranes.

Supporting Information Available

Additional analyses of the simulations reported in this contribution. This material is available free of charge via the Internet at http://pubs.acs.org/.

Acknowledgement

We thank Dr. Chetan Raj Rupakheti for his help with the parametrization of HYL on the GAAMP server.

Funding

C.H.T. and Y.W. are supported by Project 21403183 from the National Natural Science Foundation of China and Project 14323816 from the Research Grants Council. Y.W. and C.C. acknowledge the France-Hong Kong Programme Hubert Curien (PHC) Procore for funding. Y.W. also acknowledges direct grant support from the Chinese University of Hong Kong. This work was also supported in part by the Special Program for Applied Research on Super Computation of the NSFC-Guangdong Joint Fund (the second phase). J.C. acknowledges support from the U.S. National Science Foundation (Grant CHE-1726332).

References

- (1) Sliwoski, G.; Kothiwale, S.; Meiler, J.; Lowe, E. W. Computational Methods in Drug Discovery. *Pharmacological Reviews* **2013**, *66*, 334–395.
- (2) Bowes, J.; Brown, A. J.; Hamon, J.; Jarolimek, W.; Sridhar, A.; Waldron, G.; Whitebread, S. Reducing safety-related drug attrition: the use of in vitro pharmacological profiling. *Nature Reviews Drug Discovery* **2012**, *11*, 909–922.

- (3) Tsaioun, K.; Bottlaender, M.; and, A. M. ADDME Avoiding Drug Development Mistakes Early: central nervous system drug discovery perspective. *BMC Neurology* **2009**, *9*, S1.
- (4) Kansy, M.; Senner, F.; Gubernator, K. Physicochemical High Throughput Screening: Parallel Artificial Membrane Permeation Assay in the Description of Passive Absorption Processes. *Journal of Medicinal Chemistry* **1998**, *41*, 1007–1010.
- (5) Madin, S.; Darby Jr, N. Established kidney cell lines of normal adult bovine and ovine origin. *Proceedings of the Society for Experimental Biology and Medicine* **1958**, 98, 574–576.
- (6) Irvine, J. D.; Takahashi, L.; Lockhart, K.; Cheong, J.; Tolan, J. W.; Selick, H.; Grove, J. R. MDCK (Madin-Darby canine kidney) cells: A tool for membrane permeability screening. *Journal of pharmaceutical sciences* 1999, 88, 28–33.
- (7) Needham, D.; Zhelev, D. *Perspectives in Supramolecular Chemistry*; John Wiley & Sons, Ltd., pp 102–147.
- (8) Xiang, T.; Anderson, B. The relationship between permeant size and permeability in lipid bilayer membranes. *The Journal of Membrane Biology* **1994**, *140*.
- (9) Walter, A.; Gutknecht, J. Permeability of small nonelectrolytes through lipid bilayer membranes. *The Journal of Membrane Biology* **1986**, *90*, 207–217.
- (10) Bemporad, D.; Luttmann, C.; Essex, J. Computer Simulation of Small Molecule Permeation across a Lipid Bilayer: Dependence on Bilayer Properties and Solute Volume, Size, and Cross-Sectional Area. *Biophysical Journal* **2004**, *87*, 1–13.
- (11) Lande, M. B. The relationship between membrane fluidity and permeabilities to water, solutes, ammonia, and protons. *The Journal of General Physiology* **1995**, *106*, 67–84.
- (12) Mathai, J. C.; Tristram-Nagle, S.; Nagle, J. F.; Zeidel, M. L. Structural Determinants of Water Permeability through the Lipid Membrane. *The Journal of General Physiology* 2007, 131, 69–76.

- (13) Xiang, T.; Anderson, B. Permeability of acetic acid across gel and liquid crystalline lipid bilayers conforms to free surface area theory. *Biophysical Journal* **1997**, 72, 223–237.
- (14) Dearden, J. C. In silico prediction of drug toxicity. *J. Comput. Aided Mol. Des.* **2003**, *17*, 119–127.
- (15) Lee, C. T.; Comer, J.; Herndon, C.; Leung, N.; Pavlova, A.; Swift, R. V.; Tung, C.; Rowley, C. N.; Amaro, R. E.; Chipot, C.; Wang, Y.; Gumbart, J. C. Simulation-Based Approaches for Determining Membrane Permeability of Small Compounds. *Journal of Chemical Information and Modeling* 2016, 56, 721–733.
- (16) Dickson, C. J.; Hornak, V.; Pearlstein, R. A.; Duca, J. S. Structure–Kinetic Relationships of Passive Membrane Permeation from Multiscale Modeling. *Journal of the American Chemical Society* 2016, 139, 442–452.
- (17) Sun, R.; Dama, J. F.; Tan, J. S.; Rose, J. P.; Voth, G. A. Transition-Tempered Metadynamics Is a Promising Tool for Studying the Permeation of Drug-like Molecules through Membranes. *Journal of Chemical Theory and Computation* **2016**, *12*, 5157–5169.
- (18) Bennion, B. J.; Be, N. A.; McNerney, M. W.; Lao, V.; Carlson, E. M.; Valdez, C. A.; Malfatti, M. A.; Enright, H. A.; Nguyen, T. H.; Lightstone, F. C.; Carpenter, T. S. Predicting a Drug's Membrane Permeability: A Computational Model Validated With in Vitro Permeability Assay Data. *The Journal of Physical Chemistry B* 2017, 121, 5228–5237.
- (19) Marrink, S.-J.; Berendsen, H. J. C. Simulation of water transport through a lipid membrane. *The Journal of Physical Chemistry* **1994**, *98*, 4155–4168.
- (20) Torrie, G.; Valleau, J. Nonphysical sampling distributions in Monte Carlo free-energy estimation: Umbrella sampling. *Journal of Computational Physics* **1977**, *23*, 187–199.
- (21) Darve, E.; Rodríguez-Gómez, D.; Pohorille, A. Adaptive biasing force method for scalar and vector free energy calculations. *The Journal of Chemical Physics* **2008**, *128*, 144120.

- (22) Comer, J.; Gumbart, J. C.; Hénin, J.; Lelièvre, T.; Pohorille, A.; Chipot, C. The Adaptive Biasing Force Method: Everything You Always Wanted To Know but Were Afraid To Ask. *The Journal of Physical Chemistry B* **2015**, *119*, 1129–1151.
- (23) Laio, A.; Parrinello, M. Escaping free-energy minima. *Proceedings of the National Academy of Sciences* **2002**, *99*, 12562–12566.
- (24) Allen, M. P.; Tildesley, D. J. Computer Simulation of Liquids; Oxford University Press, 1987.
- (25) Woolf, T. B.; Roux, B. Conformational Flexibility of o-Phosphorylcholine and o-Phosphorylethanolamine: A Molecular Dynamics Study of Solvation Effects. *Journal of the American Chemical Society* **1994**, *116*, 5916–5926.
- (26) Hummer, G. Position-dependent diffusion coefficients and free energies from Bayesian analysis of equilibrium and replica molecular dynamics simulations. *New Journal of Physics* **2005**, 7, 34–34.
- (27) Gaalswyk, K.; Awoonor-Williams, E.; Rowley, C. N. Generalized Langevin Methods for Calculating Transmembrane Diffusivity. *Journal of Chemical Theory and Computation* **2016**, *12*, 5609–5619.
- (28) Mamonov, A. B.; Kurnikova, M. G.; Coalson, R. D. Diffusion constant of K inside Gramicidin A: A comparative study of four computational methods. *Biophysical Chemistry* **2006**, *124*, 268–278.
- (29) Comer, J.; Chipot, C.; González-Nilo, F. D. Calculating Position-Dependent Diffusivity in Biased Molecular Dynamics Simulations. *Journal of Chemical Theory and Computation* **2013**, 9, 876–882.
- (30) Chipot, C.; Comer, J. Subdiffusion in Membrane Permeation of Small Molecules. *Scientific Reports* **2016**, *6*.

- (31) Comer, J.; Schulten, K.; Chipot, C. Permeability of a Fluid Lipid Bilayer to Short-Chain Alcohols from First Principles. *Journal of Chemical Theory and Computation* **2017**, *13*, 2523–2532.
- (32) Ghaemi, Z.; Alberga, D.; Carloni, P.; Laio, A.; Lattanzi, G. Permeability Coefficients of Lipophilic Compounds Estimated by Computer Simulations. *Journal of Chemical Theory and Computation* **2016**, *12*, 4093–4099.
- (33) Ohvo-Rekilä, H. Cholesterol interactions with phospholipids in membranes. *Progress in Lipid Research* **2002**, *41*, 66–97.
- (34) Pan, J.; Mills, T. T.; Tristram-Nagle, S.; Nagle, J. F. Cholesterol Perturbs Lipid Bilayers Nonuniversally. *Physical Review Letters* **2008**, *100*.
- (35) Yeagle, P. L. Cholesterol and the cell membrane. *Biochimica et Biophysica Acta (BBA) Reviews on Biomembranes* **1985**, 822, 267–287.
- (36) Gensure, R. H.; Zeidel, M. L.; Hill, W. G. Lipid raft components cholesterol and sphin-gomyelin increase H⁺/OH⁻ permeability of phosphatidylcholine membranes. *Biochemical Journal* **2006**, *398*, 485–495.
- (37) Saito, H.; Shinoda, W. Cholesterol Effect on Water Permeability through DPPC and PSM Lipid Bilayers: A Molecular Dynamics Study. *The Journal of Physical Chemistry B* **2011**, 115, 15241–15250.
- (38) Wennberg, C. L.; van der Spoel, D.; Hub, J. S. Large Influence of Cholesterol on Solute Partitioning into Lipid Membranes. *Journal of the American Chemical Society* **2012**, *134*, 5351–5361.
- (39) Falck, E.; Patra, M.; Karttunen, M.; Hyvonen, M. T.; Vattulainen, I. Impact of cholesterol on voids in phospholipid membranes. *The Journal of Chemical Physics* **2004**, *121*, 12676.

- (40) Crank, J.; Nicolson, P.; Hartree, D. R. A practical method for numerical evaluation of solutions of partial differential equations of the heat-conduction type. *Mathematical Proceedings* of the Cambridge Philosophical Society **1947**, 43, 50.
- (41) Sweilam, N.; Khader, M.; Mahdy, A. Crank-Nicolson finite difference method for solving time-fractional diffusion equation. *Journal of Fractional Calculus and Applications* **2012**, 2, 1–9.
- (42) Murio, D. A. Implicit finite difference approximation for time fractional diffusion equations. *Computers & Mathematics with Applications* **2008**, *56*, 1138–1145.
- (43) Phillips, J. C.; Braun, R.; Wang, W.; Gumbart, J.; Tajkhorshid, E.; Villa, E.; Chipot, C.; Skeel, R. D.; Kalé, L.; Schulten, K. Scalable molecular dynamics with NAMD. *Journal of Computational Chemistry* **2005**, *26*, 1781–1802.
- (44) Klauda, J. B.; Venable, R. M.; Freites, J. A.; O'Connor, J. W.; Tobias, D. J.; Mondragon-Ramirez, C.; Vorobyov, I.; MacKerell, A. D.; Pastor, R. W. Update of the CHARMM All-Atom Additive Force Field for Lipids: Validation on Six Lipid Types. *The Journal of Physical Chemistry B* 2010, 114, 7830–7843.
- (45) Jorgensen, W. L.; Chandrasekhar, J.; Madura, J. D.; Impey, R. W.; Klein, M. L. Comparison of simple potential functions for simulating liquid water. *The Journal of Chemical Physics* 1983, 79, 926–935.
- (46) Feller, S. E.; Zhang, Y.; Pastor, R. W.; Brooks, B. R. Constant pressure molecular dynamics simulation: The Langevin piston method. *The Journal of Chemical Physics* **1995**, *103*, 4613–4621.
- (47) Andersen, H. C. Rattle: A "velocity" version of the shake algorithm for molecular dynamics calculations. *Journal of Computational Physics* **1983**, *52*, 24–34.

- (48) Miyamoto, S.; Kollman, P. A. Settle: An analytical version of the SHAKE and RATTLE algorithm for rigid water models. *Journal of Computational Chemistry* **1992**, *13*, 952–962.
- (49) Tuckerman, M.; Berne, B. J.; Martyna, G. J. Reversible multiple time scale molecular dynamics. *The Journal of Chemical Physics* **1992**, *97*, 1990–2001.
- (50) Miller, G. W.; Schnellmann, R. G. Cytoprotection by inhibition of chloride channels: the mechanism of action of glycine and strychnine. *Life Sciences* **1993**, *53*, 1211–1215.
- (51) Piper, A. S.; Greenwood, I. A. Anomalous effect of anthracene-9-carboxylic acid on calcium-activated chloride currents in rabbit pulmonary artery smooth muscle cells. *British Journal of Pharmacology* **2003**, *138*, 31–38.
- (52) Herdewijn, P.; Pauwels, R.; Baba, M.; Balzarini, J.; De Clercq, E. Synthesis and anti-HIV activity of various 2'-and 3'-substituted 2', 3'-dideoxyadenosines: a structure-activity analysis. *Journal of Medicinal Chemistry* **1987**, *30*, 2131–2137.
- (53) Vanommeslaeghe, K.; Hatcher, E.; Acharya, C.; Kundu, S.; Zhong, S.; Shim, J.; Darian, E.; Guvench, O.; Lopes, P.; Vorobyov, I.; MacKerell, A. D. CHARMM general force field: A force field for drug-like molecules compatible with the CHARMM all-atom additive biological force fields. *Journal of Computational Chemistry* 2010, 31, 671–690.
- (54) Vanommeslaeghe, K.; MacKerell Jr, A. D. Automation of the CHARMM General Force Field (CGenFF) I: bond perception and atom typing. *Journal of Chemical Information and Modeling, volume=52, number=12, pages=3144–3154, year=2012, publisher=ACS Publications*
- (55) Vanommeslaeghe, K.; Raman, E. P.; MacKerell Jr, A. D. Automation of the CHARMM General Force Field (CGenFF) II: assignment of bonded parameters and partial atomic charges. *Journal of Chemical Information and Modeling* **2012**, *52*, 3155–3168.
- (56) Landau, L. D. Statistical Physics; Clarendon Press: Oxford, 1938.

- (57) Zwanzig, R. W. High-Temperature Equation of State by a Perturbation Method. I. Nonpolar Gases. *The Journal of Chemical Physics* **1954**, 22, 1420–1426.
- (58) Mayne, C. G.; Saam, J.; Schulten, K.; Tajkhorshid, E.; Gumbart, J. C. Rapid parameterization of small molecules using the force field toolkit. *Journal of Computational Chemistry* **2013**, 34, 2757–2770.
- (59) Humphrey, W.; Dalke, A.; Schulten, K. VMD Visual Molecular Dynamics. **1996**, *14*, 33–38.
- (60) Bennett, W. F. D.; Hong, C. K.; Wang, Y.; Tieleman, D. P. Antimicrobial Peptide Simulations and the Influence of Force Field on the Free Energy for Pore Formation in Lipid Bilayers. *Journal of Chemical Theory and Computation* **2016**, *12*, 4524–4533.
- (61) Comer, J.; Schulten, K.; Chipot, C. Calculation of Lipid-Bilayer Permeabilities Using an Average Force. *Journal of Chemical Theory and Computation* **2014**, *10*, 554–564.
- (62) Darve, E.; Pohorille, A. Calculating free energies using average force. *The Journal of Chemical Physics* **2001**, *115*, 9169–9183.
- (63) Hénin, J.; Chipot, C. Overcoming free energy barriers using unconstrained molecular dynamics simulations. *The Journal of Chemical Physics* **2004**, *121*, 2904–2914.
- (64) von Toussaint, U. Bayesian inference in surface physics. *Reviews of Modern Physics* **2011**, 83, 943–999.
- (65) Bennett, W. F. D.; MacCallum, J. L.; Tieleman, D. P. Thermodynamic Analysis of the Effect of Cholesterol on Dipalmitoylphosphatidylcholine Lipid Membranes. *Journal of the American Chemical Society* **2009**, *131*, 1972–1978.
- (66) Palacios, L. E.; Wang, T. Egg-yolk lipid fractionation and lecithin characterization. *Journal of the American Oil Chemists' Society* **2005**, 82, 571–578.

- (67) Leekumjorn, S.; Sum, A. K. Molecular characterization of gel and liquid-crystalline structures of fully hydrated POPC and POPE bilayers. *The Journal of Physical Chemistry B* **2007**, *111*, 6026–6033.
- (68) Xiang, T.-X.; Chen, X.; Anderson, B. D. Transport methods for probing the barrier domain of lipid bilayer membranes. *Biophysical Journal* **1992**, *63*, 78–88.
- (69) Aksimentiev, A.; Schulten, K. Imaging α-Hemolysin with Molecular Dynamics: Ionic Conductance,Osmotic Permeability, and the Electrostatic Potential Map. *Biophysical Journal* 2005, 88, 3745–3761.
- (70) Tieleman, D. P. *BMC Biochemistry* **2004**, *5*, 10.
- (71) Cardenas, A. E.; Elber, R. Modeling kinetics and equilibrium of membranes with fields: Milestoning analysis and implication to permeation. *The Journal of Chemical Physics* **2014**, *141*, 054101.
- (72) Flenner, E.; Das, J.; Rheinstädter, M. C.; Kosztin, I. Subdiffusion and lateral diffusion coefficient of lipid atoms and molecules in phospholipid bilayers. *Physical Review E* **2009**, *79*, 011907.
- (73) Róg, T.; Stimson, L. M.; Pasenkiewicz-Gierula, M.; Vattulainen, I.; Karttunen, M. Replacing the Cholesterol Hydroxyl Group with the Ketone Group Facilitates Sterol Flip-Flop and Promotes Membrane Fluidity. *The Journal of Physical Chemistry B* **2008**, *112*, 1946–1952.
- (74) Bennett, W. F. D.; MacCallum, J. L.; Hinner, M. J.; Marrink, S. J.; Tieleman, D. P. Molecular View of Cholesterol Flip-Flop and Chemical Potential in Different Membrane Environments. *Journal of the American Chemical Society* 2009, 131, 12714–12720.
- (75) Jo, S.; Rui, H.; Lim, J. B.; Klauda, J. B.; Im, W. Cholesterol Flip-Flop: Insights from Free Energy Simulation Studies. *The Journal of Physical Chemistry B* **2010**, *114*, 13342–13348.

- (76) Kučerka, N.; Tristram-Nagle, S.; Nagle, J. F. Structure of Fully Hydrated Fluid Phase Lipid Bilayers with Monounsaturated Chains. *Journal of Membrane Biology* **2006**, *208*, 193–202.
- (77) Menichetti, R.; Kanekal, K. H.; Kremer, K.; Bereau, T. In silico screening of drug-membrane thermodynamics reveals linear relations between bulk partitioning and the potential of mean force. *The Journal of Chemical Physics* **2017**, *147*, 125101.
- (78) Harder, E.; MacKerell Jr, A. D.; Roux, B. Many-body polarization effects and the membrane dipole potential. *Journal of the American Chemical Society* **2009**, *131*, 2760–2761.
- (79) Li, H.; Chowdhary, J.; Huang, L.; He, X.; MacKerell Jr, A. D.; Roux, B. Drude polarizable force field for molecular dynamics simulations of saturated and unsaturated zwitterionic lipids. *Journal of Chemical Theory and Computation* **2017**, *13*, 4535–4552.
- (80) Ghaemi, Z.; Minozzi, M.; Carloni, P.; Laio, A. A novel approach to the investigation of passive molecular permeation through lipid bilayers from atomistic simulations. *Journal of Physical Chemistry B* **2012**, *116*, 8714–8721.

Graphical TOC Entry

